Twelve Times Smaller Limit on the Electric Dipole Moment of the Electron

The ACME Collaboration, J. Baron[2], W. Campbell[3], D. DeMille[1], J. Doyle[2], G. Gabrielse[2], Y. V. Gurevich[1], P. W. Hess[2], N. R. Hutzler[2], E. Kirilov[4], B. R. O'Leary[1], C. Panda[2], E. S. Petrik[2], B. Spaun[2], A. Vutha[5], and A. D. West[1]

Abstract:

The Standard Model (SM) of particle physics is known to be incomplete. It fails to explain numerous observational facts such as the existence of dark matter, and the fact that a small amount of matter survived annihilation with antimatter following the big bang. Many proposed extensions to the SM, such as weak-scale Supersymmetry (SUSY), provide explanations for these phenomena by positing the existence of new particles and new interactions that break symmetry under time-reversal (T). These same theories nearly always predict a small, yet potentially measureable electric dipole moment (EDM) of the electron (which is also asymmetric under T), typically in the range of $10^{-27} - 10^{-30}$ e cm. Despite over six decades of experimental searching[1], no EDM of any fundamental particle has been measured. Here, we report a new search for the electron EDM, d_e, in the polar molecule thorium monoxide (ThO). Our result, $d_e = (2.1 \pm 3.7_{\rm stat} \pm 2.5_{\rm syst}) \times 10^{-29}$ e cm , corresponds to an upper limit of $|d_e| < 8.8 \times 10^{-29}$ e cm with 90 percent confidence, an order of magnitude improvement in sensitivity compared to the previous best limit[2]. Our result sets strong constraints on new physics associated with T-violating interactions at the TeV energy scale. Standard Model extensions that predict a d_e above this limit must therefore be abandoned or have their parameters fine-tuned to lower their d_e prediction.

The exceptionally high internal effective electric field ($\mathcal{E}_{\rm eff}$) of heavy neutral atoms and molecules can be used to precisely probe for d_e, via the energy shift $U = -\vec{d}_e \cdot \vec{\mathcal{E}}_{\rm eff} = -2 d_e \vec{S} \cdot \vec{\mathcal{E}}_{\rm eff}$, where $\vec{S}$ is the spin of the electron. Valence electrons in the molecule travel relativistically near the heavy nucleus, enhancing $\mathcal{E}_{\rm eff}$ up to a value that is 10^6 times larger than any static laboratory field[3,4]. Such enhancements have produced the previous best limits on d_e in experiments with thallium (Tl) atoms[5], 1.6×10^{-27} e cm, and ytterbium fluoride (YbF) molecules[2,6], 1.05×10^{-27} e cm. Molecules have numerous advantages over atoms. Molecules can be aligned in more modest electric fields, significantly lowering unwanted spurious experimental effects. Molecular internal state structure can suppress the motional electric fields and geometric phases that ultimately limited the Tl measurement, as demonstrated by the YbF experiment[2]. (Ref[7] has proposed a new class of atoms with some suppression properties.) For molecules with nonzero orbital angular momentum, $\mathcal{E}_{\rm eff}$ can be reversed by tuning a laser without reversing the laboratory electric field, as demonstrated by the lead oxide (PbO) experiment[8,9]. This allows for an additional level of systematic error suppression and checks for spurious effects. An advantage of ThO over YbF and PbO is its near-vanishing magnetic moment in the $^3\Delta_1$ metastable state, which provides great insensitivity to uncontrolled magnetic fields[10,11].

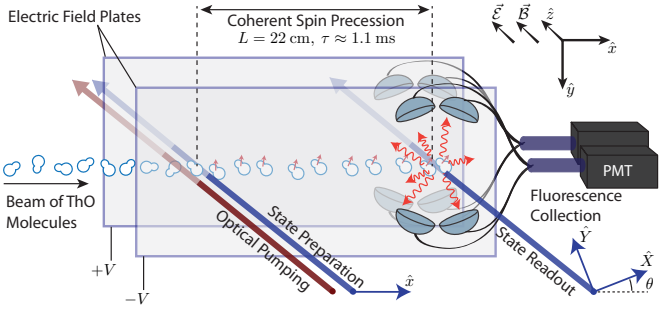

FIG. 1. Schematic of the apparatus. A collimated pulse of ThO molecules enters a magnetically shielded region. An aligned spin state, prepared via optical pumping, precesses in applied electric and magnetic fields. The final spin alignment is read out by a laser with rapidly alternating linear polarizations, $\hat{X}, \hat{Y}$, with the resulting fluorescence collected and detected with photomultiplier tubes (PMTs).

To measure the electron EDM we perform a spin precession measurement on a molecular beam of ^{232}Th^{16}O. A pulse of ThO molecules from a cryogenic buffer gas beam source[12,13] (see Methods) passes between parallel electric field plates (figure 1). Coherent superpositions of two ThO spin states are prepared using optical pumping and state preparation lasers. Parallel electric ($\vec{\mathcal{E}}$) and magnetic ($\vec{\mathcal{B}}$) fields (the latter from external coils not shown) interact with the electric and magnetic dipole moments, causing energy shifts that change sign when the either the field directions or the orientation of the molecules are reversed. These shifts cause the two states to accumulate a relative phase as they travel through the parallel fields. This phase is measured with a readout laser and detected via fluorescence. The difference in phases between measurements with $\mathcal{E}_{\rm eff}$ reversed (which can be accomplished by reversing either E or the molecule orientation) is proportional to d_e with a calculated proportionality constant[14,15].

In more detail, molecules pass through a laser region that optically pumps them from the ground electronic state into the ground rotational level, $J = 1$, of the metastable electronic $H^3\Delta_1$ state manifold, in an incoherent mixture of the $\tilde{\mathcal{N}} = \pm 1$, $M = \pm 1$ states. M is the angular momentum projection along the $\hat{z}$ axis. $\tilde{\mathcal{N}} = {\rm sign}(\vec{\mathcal{E}} \cdot \hat{n})$ is the direction of the induced molecular electric dipole moment, $D\hat{n}$, with respect to $\vec{\mathcal{E}}$, when $\mathcal{E} \gtrsim 1$ V/cm[11]. The molecules then enter a linearly polarized state-preparation laser beam, whose frequency is set on resonance at 1090 nm between $H \rightarrow C$. The C state is a short-lived electronic state within which there are two opposite parity $\tilde{\mathcal{P}} = \pm 1$ states with $J = 1, M = 0$. The laser frequency determines the $\tilde{\mathcal{N}}, \tilde{\mathcal{P}}$ states that are addressed for a given spin precession measurement. This laser optically pumps the *bright* superposition of the two resonant $M = \pm 1$ sublevels out of the H state, leaving behind the *dark* orthogonal superposition. If the state preparation laser is polarized along the $\hat{x}$ axis, the prepared state, $|\psi(\hat{x}, \tau = 0), \tilde{\mathcal{N}}\rangle$, has the electron spin aligned along the $\hat{y}$ axis. The spin then precesses in the xy

[1]Department of Physics, Yale University, 217 Prospect Street, New Haven, Connecticut 06511, USA. [2]Department of Physics, Harvard University, 17 Oxford Street, Cambridge, Massachusetts 02138, USA [3]Department of Physics and Astronomy, UCLA, 475 Portola Plaza, Los Angeles, CA 90095, USA. [4]Institut für Experimentalphysik, Universität Innsbruck, Technikerstrasse 25/4, A-6020 Innsbruck, Austria. [5]Department of Physics and Astronomy, York University, 128 Petrie Science and Engineering Building, 4700 Keele Street, Toronto, Ontario M3J 1P3, Canada.

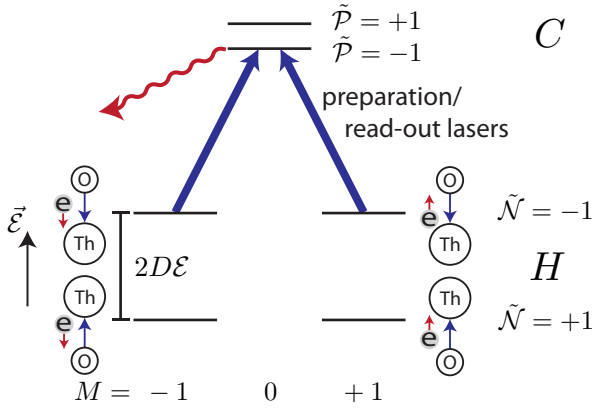

FIG. 2. Energy level diagram showing the relevant states. The state-preparation and read-out lasers drive one molecule orientation $\tilde{\mathcal{N}}=\pm1$ (split by $2D\mathcal{E}\sim 100$ MHz) in the H state to C, with parity $\tilde{\mathcal{P}}=\pm1$ (split by 50 MHz). Population in the C state decays via spontaneous emission, and we detect the resulting fluorescence. H state levels are accompanied by cartoons displaying the orientation of the effective electric field (blue arrows) and the spin of the electron (red arrows) that dominantly contributes to the d_e shift.

plane by angle ϕ to

$$|\psi(\hat{x},\tau),\tilde{\mathcal{N}}\rangle=(e^{-i\phi}|M=+1,\tilde{\mathcal{N}}\rangle+e^{+i\phi}|M=-1,\tilde{\mathcal{N}}\rangle)/\sqrt{2} \quad (1)$$

The value of the phase, ϕ, is determined by the magnitude of the projection of $\vec{\mathcal{B}}$ onto $\vec{\mathcal{E}}$, $|\mathcal{B}_z|=|\vec{\mathcal{B}}\cdot\hat{\mathcal{E}}|$ and its sign, $\tilde{\mathcal{B}}=\mathrm{sgn}(\vec{\mathcal{B}}\cdot\vec{z})$, and the electron's EDM, d_e,

$$\phi\approx-(\mu_B g\tilde{\mathcal{B}}\,|\mathcal{B}_z|+\tilde{\mathcal{N}}\tilde{\mathcal{E}}d_e\mathcal{E}_{\mathrm{eff}})\tau/\hbar \quad (2)$$

where $\tilde{\mathcal{E}}\equiv\mathrm{sgn}(\vec{\mathcal{E}}\cdot\hat{z})$, $\mu_B g$ is the magnetic moment and τ is the spin precession time.[16] The sign of the EDM term, $\tilde{\mathcal{N}}\tilde{\mathcal{E}}$, is derived from the relative orientation between internal electric field and the electron spin projection as illustrated in figure 2.

After precessing over a distance of $L\approx 22$ cm (corresponding to $\tau\approx 1.1$ ms), we measure ϕ by optically pumping on the same $H\rightarrow C$ transition with the state readout laser. The laser polarization rapidly alternates between $\hat{X}$ and $\hat{Y}$ and we record the fluorescence from the decay of C to the ground state (see Methods). This procedure amounts to projective measurements of the molecule alignment onto $\hat{X}$ and $\hat{Y}$, which are defined such that $\hat{X}$ is at an angle θ with respect to $\hat{x}$ in the xy plane. This polarization switching results in modulated fluorescence signals S_X and S_Y. To normalize our measurement to molecule number fluctuations, we compute the asymmetry,[10]

$$\mathcal{A}\equiv\frac{S_X-S_Y}{S_X+S_Y}=\mathcal{C}\cos\left(2\left(\phi-\theta\right)\right) \quad (3)$$

where $\mathcal{C}$ is the contrast, a number that encodes our sensitivity to phase. We set $|\mathcal{B}_z|$ and θ such that $\phi-\theta\approx\frac{\pi}{4}(2n+1)$ for integer n, so that the asymmetry is linearly proportional to small changes in ϕ, and maximally sensitive to the EDM. We measure the contrast, $|\mathcal{C}|=94\pm2\%$, by dithering θ between two nearby values that differ by 0.1 rad denoted by $\tilde{\theta}=\pm1$. This procedure allows us to extract a measurement of ϕ.

We perform this spin precession measurement repeatedly under varying experimental conditions in order to (a) distinguish the EDM energy shift from background phases and (b) search for and monitor possible systematic errors. Within a *block* of data taken over 40 s, we perform 4 identical measurements of the phase for each of a complete set of 2^4 experimental states derived from 4 binary switches, listed from fastest (.5 s) to slowest (20 s): the molecule alignment, $\tilde{\mathcal{N}}$; the direction of the applied electric field, $\tilde{\mathcal{E}}$; the read-out laser polarization dither state, $\tilde{\theta}$; and the magnetic field direction, $\tilde{\mathcal{B}}$. These reversals are important for the measurement because the EDM energy shift is odd under the $\tilde{\mathcal{N}}$ and $\tilde{\mathcal{E}}$ switches, the $\tilde{\theta}$ switch is required to measure $\mathcal{C}$, and the $\tilde{\mathcal{B}}$ switch is required to measure τ. For each $(\tilde{\mathcal{N}},\tilde{\mathcal{E}},\tilde{\mathcal{B}})$ state of the experiment, we measure $\mathcal{A}$ and $\mathcal{C}$ from which we can extract ϕ. For data from each block, we form 'parity components' of the phase, ϕ^p, which are combinations of the measured phases that are odd or even under these switch operations[9,17]. We denote the experimental parity of a quantity with a superscript, listing the switch labels under which the quantity is odd; it is even under all unlabelled switches. These "parity components" correspond to particular physical effects that contribute to ϕ. For example, we extract the EDM from the $\phi^{\mathcal{NE}}$ component of phase, which is odd under the $\tilde{\mathcal{N}}$ and $\tilde{\mathcal{E}}$ switches and even under the $\tilde{\mathcal{B}}$ switch, and we extract the mean precession time τ from the component of phase that is odd under only the $\tilde{\mathcal{B}}$ switch, $\phi^{\mathcal{B}}=-\mu_B g\,|\mathcal{B}_z|\,\tau/\hbar$. We then compute the frequency, $\omega^p\equiv\phi^p/\tau$, and extract the EDM measurement from $d_e=-\hbar\omega^{\mathcal{NE}}/\mathcal{E}_{\mathrm{eff}}$.

On a slower time scale, from block to block, we perform additional *superblock* binary switches that are useful in the suppression of some known systematic errors and in the search for unknown ones. These switches, which occur on the 40-1200 s time scales, are: (1) the excited state parity addressed by the state read-out lasers, $\tilde{\mathcal{P}}$; (2) a rotation of the read-out polarization basis by $\theta\rightarrow\theta+\pi/2$, $\tilde{\mathcal{R}}$; (3) a reversal of the leads that supply the electric fields, $\tilde{\mathcal{L}}$; and (4) a global polarization rotation of both the state preparation and read-out laser polarizations, $\tilde{\mathcal{G}}$. Both the $\tilde{\mathcal{P}}$ and $\tilde{\mathcal{R}}$ switches interchange the role of the $\hat{X}$ and $\hat{Y}$ readout polarization beams and hence reject systematic errors associated with a small difference in power, shape, or pointing them. The two $\tilde{\mathcal{G}}$ state angles are chosen to suppress systematics that couple to unwanted ellipticity imprinted on the polarizations by a birefringence in the electric field plates. The $\tilde{\mathcal{L}}$ switch rejects systematics that couple to an offset voltage in the electric field power supplies. We define a complete *EDM measurement* as a set of the 2^8 block and superblock states. All of our systematic checks were performed with this experimental protocol. The extracted EDM value is even under all of the superblock switches.

The total dataset consists of about 10^4 blocks of data, taken over the course of ~2 weeks. During this dataset, in addition to the 8 switches described above, we also varied, from fastest (hours) to slowest (a few days): the $\mathcal{B}-$field magnitude, $|\mathcal{B}_z|\approx 1,\ 20,\ 40$ mG (corresponding to $|\phi|\approx 0,\frac{\pi}{4},\frac{\pi}{2}$ respectively), the $\mathcal{E}$-field magnitude $|\mathcal{E}_z|\approx 36,\ 142$ V/cm, and the pointing direction of the lasers, $\hat{k}\cdot\hat{z}=\pm1$. Previous EDM experiments have been unable to operate at multiple electric fields due to incomplete atomic/molecular polarization. figure 3b shows measured EDM values obtained when the dataset is grouped according to the states of $|\mathcal{B}_z|\,,|\mathcal{E}_z|$, $\hat{k}\cdot\hat{z}$, and each superblock switch. All of these measurements are consistent with the measured mean within $\sim 1\sigma$. We also performed periodic auxilliary measurements during this dataset to monitor the dominant systematics errors, described below.

We compute the standard error in the mean and use standard gaussian error propagation to obtain the reported statistical uncertainty. The reported upper limit is computed using the Feldman-Cousins prescription[18] applied to a folded normal distribution at 90% confidence. To prevent experimental bias, we performed a blind analysis by adding an unknown offset to the EDM measurement. We revealed this offset only after data collection, data cuts, and error analysis procedures were complete. Our statisti-

cal distribution is consistent with a gaussian; Figure 3a shows a histogram of EDM measurements grouped by block and by time within the molecular beam pulse. When fit to a constant value, the reduced chi-squared is $\chi^2 = .996 \pm .006$. Despite the empirical gaussianity of the data, the asymmetry, $\mathcal{A}$, obeys a ratio distribution, which has large non-gaussian tails in the limit of low signal to noise[19]. We apply a photon count rate threshold cut to the data so that we only include data with a large signal-to-noise ratio, resulting in a statistical distribution that approximates a gaussian. Based on the total number of detected photons that contribute to the measurement, we determine that the error in our measurement is 1.15 times that from photo-electron shot noise in the PMTs.[16]

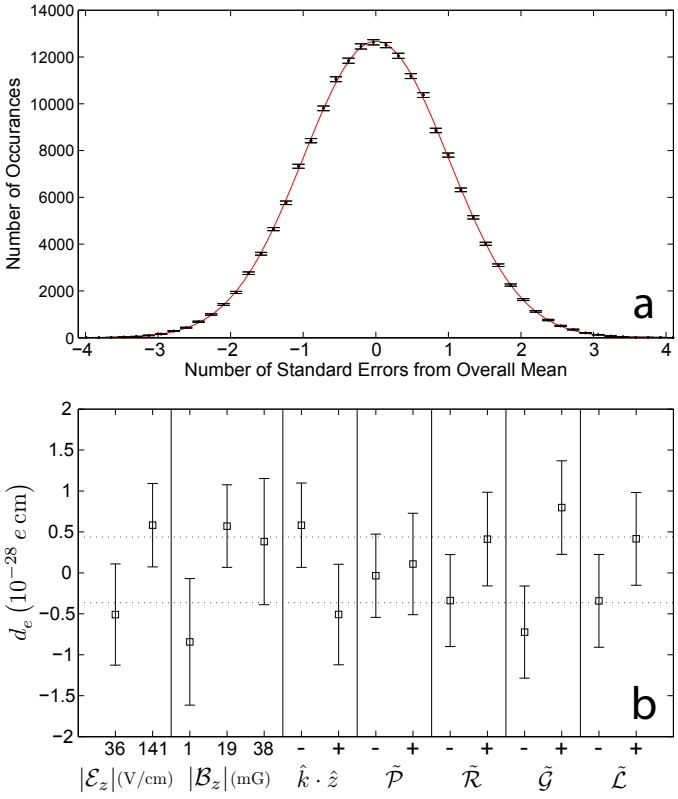

FIG. 3. **a.** Statistical distribution of EDM measurements grouped by block and time within molecule pulse. Errorbars represent expected fluctuations in each histogram bin. **b.** Measured EDM values grouped by the states of $|\mathcal{B}_z|$, $|\mathcal{E}_z|$, $\hat{k}\cdot\hat{z}$, and each superblock switch.

To search for possible sources of systematic error, we tuned over 40 separate parameters and measured their effect on d_e and many other components of the phase correlated with $\tilde{\mathcal{N}}$, $\tilde{\mathcal{E}}$, or $\tilde{\mathcal{B}}$. These parameters are intentionally applied tunable imperfections in the experiment, such as transverse magnetic fields or laser detunings. The majority of parameters did not have correlations with d_e.

Assuming that d_e depends linearly on each parameter P, the possible systematic shift and uncertainty of d_e is evaluated from the measured slope, $S = \partial d_e/\partial P$, and the average and uncertainty in the parameter during normal operation (measured from auxiliary measurements). If S was not monitored throughout the data set, we do not apply a systematic correction for that parameter but simply include an upper limit in our systematic error budget. Data taken where any parameter had been tuned outside of it's nominal range was not included in the calculation of our EDM measurement before systematic corrections. Table 1 contains a list of all contributions to our systematic error.

We discovered two parameters which systematically shift the value of d_e within our experimental resolution. Both couple to the AC Stark shift induced by the lasers. The molecules are initially prepared in the dark state with a spin orientation dependent on the laser polarization. If there is a polarization gradient along the molecular beam propagation direction, the molecules acquire a small bright state amplitude. Away from the center of a Gaussian laser profile, the laser can be weak enough that the bright state amplitude is not rapidly pumped away and it acquires a phase relative to the dark state due to their mutual energy splitting, the AC Stark shift. An equivalent phase is acquired in the state read-out laser. These phases depend on the detuning Δ of (relative to) the $H \to C$ resonance and the Rabi frequency Ω_r (proportional to the AC electric field of the laser beam). This effect results in a change in the measured phase by amount $\phi_\mathrm{AC}(\Delta, \Omega_\mathrm{r}) = \alpha\Delta + \beta\Omega_\mathrm{r}$. The couplings α and β are measured directly by varying laser detuning and intensity. They depend on the spatial intensity profile and the polarization gradient. These measurements are in good agreement with our analytic and numerical models.

A significant polarization gradient can be caused by laser-induced thermal stress birefringence in the electric field plates. The lasers are elongated perpendicular to the molecular beam axis, which creates an asymmetric thermal gradient and defines the axes for the resulting birefringence gradient. By aligning the laser polarization with the birefringence axes, the polarization gradient can be minimized. We verified this both with direct gradient polarimetry[20] and through the resulting AC Stark shift systematic (figure 4a).

Such AC Stark shift effects can cause a systematic shift in our measurement of d_e if the detuning or Rabi frequency is correlated with $\tilde{\mathcal{N}}\tilde{\mathcal{E}}$. We observe both possibilities.

In addition to the ideally reversing component, $|\mathcal{E}_z|\tilde{\mathcal{E}}$, our electric field contains a non-reversing component $\mathcal{E}^\mathrm{nr}$ from voltage offsets and patch potentials. The $\mathcal{E}^\mathrm{nr}$ creates a correlated DC Stark shift and an associated detuning $\Delta^{\mathcal{N}\mathcal{E}} = D\mathcal{E}^\mathrm{nr}$. We measured $\mathcal{E}^\mathrm{nr}$ via microwave spectroscopy (figure 4b), two-photon Raman spectroscopy, and monitoring of the $\tilde{\mathcal{N}}\tilde{\mathcal{E}}$-correlated contrast.

A component of the Rabi frequency correlated with $\tilde{\mathcal{N}}\tilde{\mathcal{E}}$, $\Omega_\mathrm{r}^{\mathcal{N}\mathcal{E}}$, arises from a dependence of the Rabi frequency on the orientation of the molecular axis, $\hat{n} \approx \tilde{\mathcal{N}}\tilde{\mathcal{E}}\hat{z}$, with respect to laser propagation direction, $\hat{k}$. This $\hat{k}\cdot\hat{n}$ dependence can be caused by interference between E1 and M1 transition amplitudes on the $H \to C$ transition. Measurements of a non-zero $\tilde{\mathcal{N}}\tilde{\mathcal{E}}$-correlated fluorescence signal and an $\tilde{\mathcal{N}}\tilde{\mathcal{E}}\tilde{\mathcal{B}}$-correlated phase, both of which changed sign when we reversed $\hat{k}$, provided evidence for a nonzero $\Omega_\mathrm{r}^{\mathcal{N}\mathcal{E}}$. These channels, along with their linear dependence on an artificial $\Omega_\mathrm{r}^{\mathcal{N}\mathcal{E}}$ generated with an $\tilde{\mathcal{N}}\tilde{\mathcal{E}}$ correlated laser intensity, allowed us to measure $\Omega_\mathrm{r}^{\mathcal{N}\mathcal{E}}/\Omega_\mathrm{r} = (-8.0 \pm 0.8) \times 10^{-3}(\hat{k}\cdot\hat{z})$, where Ω_r is the uncorrelated (mean) Rabi frequency.

By intentionally exaggerating these parameters, we verified that both $\mathcal{E}^\mathrm{nr}$ and $\Omega_\mathrm{r}^{\mathcal{N}\mathcal{E}}$ could couple to AC Stark shift effects to produce a false EDM. Figure 4a illustrates our ability to suppress the measured d_e shift as a function of applied $\mathcal{E}^\mathrm{nr}$. The correlations, $\partial d_e/\partial\mathcal{E}^\mathrm{nr}$ and $\partial d_e/\partial\Omega_\mathrm{r}^{\mathcal{N}\mathcal{E}}$, were monitored at regular intervals throughout the data set. The resulting systematic corrections to d_e were all $< 1 \times 10^{-29}$ e cm.

We observed not-yet understood behavior from the $\tilde{\mathcal{N}}$-correlated phase, $\phi^\mathcal{N}$, when an $\tilde{\mathcal{N}}$-correlated laser pointing, $k^\mathcal{N}$, was present in our system. The acousto-optic modulator systems that generate the laser frequency offsets required for the $\tilde{\mathcal{N}}$ switch can produce a $k^\mathcal{N}$ of ~ 5 μrad, as measured by a laser beam profiler. We exaggerated $k^\mathcal{N}$ with mirrors mounted on electronic actuators and observed a $\phi^\mathcal{N}$ dependence on $k^\mathcal{N}$ that fluctuated

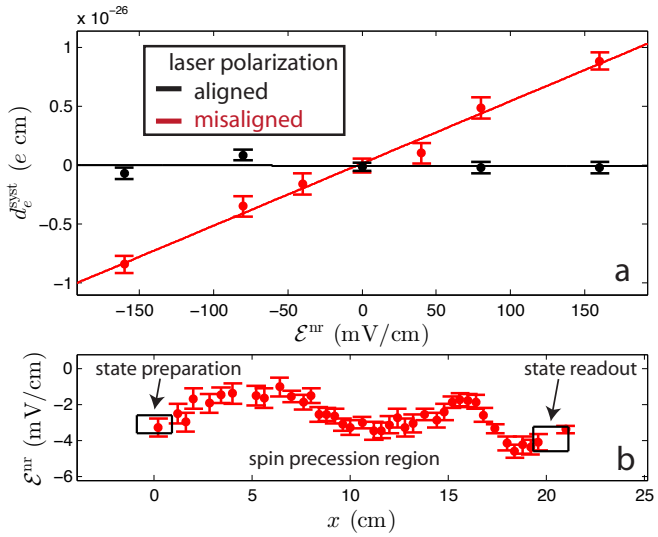

FIG. 4. **a.** Tuning out laser polarization gradient and $\partial/\partial\mathcal{E}^{\rm nr}$. The red (black) points were taken with the polarization misaligned (aligned) with the birefringence axes of the electric field plates. **b.** Microwave spectroscopic measurement of $\mathcal{E}^{\rm nr}$ along the molecule beam axis, x.

Parameter	Shift	Uncertainty
$\mathcal{E}^{\rm nr}$ correction	−6.2	5.1
Intrinsic $\Omega_{\rm r}^{\mathcal{N}\mathcal{E}}$ correction	−0.2	12.2
$\phi^{\mathcal{E}}$ correlated effects	−0.1	0.1
Pointing induced $\phi^{\mathcal{N}}$ correlation		9.7
Non-Reversing B-Field ($\mathcal{B}_z^{\rm nr}$)		6.6
Transverse B-Fields ($\mathcal{B}_x^{\rm nr}, \mathcal{B}_y^{\rm nr}$)		(0.7, 6.6)
B-Field Gradients Total (6)		9.6
Prep/Read Laser Detunings		10.2
$\mathcal{N}$ Switch Detuning		7.5
Floating E-Field $V_{\rm offset}$		1.2
Total Systematic	−6.5	24.7
Statistical		37.1
Total Uncertainty		44.6

TABLE I. Systematic and statistical errors, in units of 10^{-30} e cm. All errors are in quadrature.

significantly in time. Because we could not explain this behavior, we include in our systematic error budget any effect that might cause fluctuations in $\phi^{\mathcal{N}}$. We looked for correlations between d_e and $\phi^{\mathcal{N}}$, treating the fluctuating $\phi^{\mathcal{N}}$ channel as though it were a tunable parameter. We fit a linear slope to a plot of d_e vs $\phi^{\mathcal{N}}$, including in this plot all blocks from the published data set and from data sets where we had exaggerated $k^{\mathcal{N}}$. The resulting slope was consistent with zero and allowed us to place a systematic uncertainty limit $< 1 \times 10^{-29}$ e cm on the effect that caused $\phi^{\mathcal{N}}$ to fluctuate.

To be cautious, we also include in our systematic error budget possible contributions from effects associated with parameters that caused a non-zero d_e shift experiments similar to ours. Examples of such parameters include stray magnetic fields $\mathcal{B}_{x,y,z}^{\rm nr}$, and magnetic field gradients[9]; an $\tilde{\mathcal{E}}$-correlated phase caused by leakage current, $\vec{v}\times\vec{\mathcal{E}}$, and geometric phase effects[5]; and various laser detunings[2]. By intentionally exaggerating each of these parameters we obtained a direct d_e systematic limit of $\lesssim 10^{-29}$ e cm for each parameter. We exaggerated the $\tilde{\mathcal{E}}$-correlated phase by intentionally correlating $\mathcal{B}_z$ with $\tilde{\mathcal{E}}$, allowing us to place a $\sim 10^{-31}$ e cm limit on possible d_e shifts arising from leakage current, $\vec{v}\times\vec{\mathcal{E}}$, and geometric phase effects. We emphasize that because of our slow molecular beam, our relatively small applied electric fields, and the small magnetic dipole moment of the H state, we do not expect any of these effects to systematically shift d_e above the 10^{-32} e cm level[10,11].

The result of this first generation ThO measurement is

$$d_{\rm e} = (2.1 \pm 3.7_{\rm stat} \pm 2.5_{\rm syst}) \times 10^{-29}\ e\ {\rm cm}. \quad (4)$$

This sets a 90% confidence limit,

$$|d_e| < 8.8 \times 10^{-29}\ e\ {\rm cm}\ , \quad (5)$$

that is 12 times smaller than the previous limit[2,5]. Because paramagnetic molecules are sensitive to multiple CP violating effects, we actually measured $d_e + a\,C_S$, where C_S is the strength of a possible scalar-psuedoscalar coupling between the valence electrons and the nuclei. The relative sensitivity, $a = 1.5 \times 10^{-20}$ e cm, was calculated[14,15] along with $\mathcal{E}_{\rm eff}$. As is conventional, $C_S = 0$ is assumed to obtain the EDM limit. Assuming $d_e = 0$ instead gives $C_S = (1.3 \pm 3.0) \times 10^{-9}$, with a 90 percent confidence limit $|C_S| < 5.8 \times 10^{-9}$ that is 9 times smaller than the earlier limit[21].

For a measurably large EDM to exist, there must be new mechanisms for CP violation (T violation, assuming CPT invariance) beyond those in the Standard Model. Nearly every theory that extends the Standard Model includes such mechanisms. The effective strength of CP violation in a given model can be described by the sine of a complex phase, $\phi_{\rm CP}$. It is difficult to construct mechanisms that systematically suppress these phases, so theoretical model builders typically assume $\sin(\phi_{\rm CP}) \approx 1$. In this case, naïve dimensional estimates can be made for the size of the EDM, which can be calculated from Feynman diagrams including loops (where the number of loops corresponds to the order of perturbation theory at which they arise). An EDM arising from new CP-violating phenomena at energy Λ, in an n-loop diagram, will have size $d_e/e \sim (\alpha_{\rm eff}/4\pi)^n (m_e c^2/\Lambda^2)(\hbar c)^{-1}$, where $\alpha_{\rm eff}$ encodes the strength with which the electron couples to the new phenomena. An upper bound to the scale of new physics $\Lambda \approx 30$ TeV probed by the EDM arises when $\alpha = 1$ and $n = 1$. Indeed, in certain supersymmetric models (where strong mixing between particle families is allowed), our result probes this energy scale[?] . In most favored models, $\alpha_{\rm eff} \approx 1/137$ (the coupling strength of electromagnetic interactions). Then, in models where 1- or 2-loop diagrams dominate the EDM, our result can probe CP-violation at energy scales $\Lambda \approx 3$ TeV or 300 GeV, respectively. Predictions for the electron EDM in both of these possible cases have been calculated in the context of many models[22–24]; although details differ, these estimates are typical of the results. Notably, in every case our experiment is predicted to probe the same, or higher, energy scales as those explored directly at the Large Hadron Collider (LHC).

Our experiment has improved the electron EDM by a factor of 12 by pioneering the use of the ThO molecule and the first use of a cryogenic source of cold molecules for this purpose. Our metastable electronic ThO state has an enormous internal field that is easily aligned and saturated with a small laboratory field and allowed the ability to change a laser frequency to reverse the internal field (with no change in laboratory field). Simple arguments show that the energy being probed is comparable to or somewhat higher than what is currently being investigated by the LHC. A similarly large improvement in experimental sensitivity to

an electron EDM (as is expected in a second-generation ThO measurement) will either discover the long-predicted electron EDM or further constrain proposed extensions to the Standard Model and their CP-violating terms.

Methods

We create a pulsed molecular beam of ThO created using the buffer gas beam technique[12,13,25] operating at a 50 Hz repetition rate. Each packet of molecules leaving the source contains $\sim 10^{11}$ ThO molecules in the $J = 1$ rotational level of the ground electronic (X) and vibrational states, which are produced every 20 ms. The packet is $2 - 3$ ms wide and has a center of mass speed of $\sim$ 200 m/s. After leaving the cryogenic beam source chamber, the molecules travel through a microwave field resonant with the $|X; J = 1\rangle \leftrightarrow |X; J = 0\rangle$ transition and lasers resonant with the $|X; J = 2, 3\rangle \rightarrow |C; J = 1, 2\rangle$ transitions. The microwaves and optical pumping lasers push population from $|X; J = 0, 2, 3\rangle$ into the $|X; J = 1\rangle$ state leading to a ~ 2 times increase in its population. The molecules then pass through adjustable and fixed collimating apertures before entering the applied electric and magnetic fields in a magnetically shielded interaction region. A retroreflected 943 nm laser optically pumps population from the $|X; J = 1, M = \pm 1\rangle$ states to $|A; J = 0, M = 0\rangle$, which decays primarily into the $|H; J = 1\rangle$ state in which the EDM measurement is performed.

The spin precession region contains applied electric and magnetic fields, along with lasers to prepare and read our EDM state. The electric field is provided by two plates of 12.7 mm thick glass coated with a layer of indium tin oxide (ITO) on one side, and an anti-reflection coating on the other. The ITO coated sides of the plates face each other with a gap of 25 mm, and a voltage is applied to the ITO to create a uniform electric field.

The electric field was measured by performing microwave spectroscopy on the ThO molecules themselves. When the molecule pulse is between the state preparation and read-out regions, a short, 40 μs, burst of microwaves resonant with the DC Stark-shifted $|H; J = 1, M = \pm 1\rangle \rightarrow |H; J = 2, M = 0\rangle$ transitions is introduced by a microwave horn at the end of the apparatus, counterpropagating with the molecular beam. If on resonance, the microwaves drive a transition that spin-polarizes the molecules, similar to the state preparation scheme. We can then detect the spin polarization using the normal readout scheme. The microwave transition width is ~ 5 kHz (dominated by Doppler broadening), so the H-state dipole moment of $D \approx 1$ MHz/(V/cm)[11] (for $J = 1$) means that this method is sensitive to $\sim$ mV/cm electric field deviations with spatial resolution of $\approx$ 1 cm. Our measurement indicated that the spatial variation of the electric field is in very good agreement with the predicted electric field based on interferometric measurements of the plate spacing[26].

We can also test how well the electric field reverses by mapping the field with equal and opposite voltages on the plates. This measurement indicated that the "non-reversing" component of the electric field had magnitude $|\mathcal{E}^{\rm nr}| \approx 1 - 5$ mV/cm across the entire molecular precession region, as shown in figure 4b. This value is crucial for quantitatively understanding one of our light shift systematic errors.

The EDM measurement is performed in a vacuum chamber surrounded by five layers of mu-metal shielding. The applied magnetic field is supplied by a cosine-theta coil, with several shim coils to create a more uniform magnetic field within the precession region, and to allow us to apply transverse magnetic fields and gradients for systematic checks. Changes in the magnetic field are monitored by four 3-axis fluxgate magnetometers inside the magnetic shields, and the magnetic fields were mapped out before and after the experimental dataset was taken by sliding a 3-axis fluxgate down the beamline.

The lasers travel through the electric field plates, so all stages of the spin precession measurement are performed inside the uniform electric field. All lasers in the experiment originate from an external cavity diode laser (ECDL), frequency stabilized via an Invar transfer cavity to a CW Nd:YAG laser locked to a molecular iodine transition[27]. All required transition frequencies and state assignments were deteremined previously[28–30]. We measured the saturation intensities, radiative lifetimes, electric/magnetic dipole moments, and branching ratios for all required states and transitions.

In order to normalize against drifting molecular beam properties (pulse shape, total number, velocity mean and distribution, etc.), we perform a spin precession measurement every 10 μs, which is much faster than the molecular beam variations[16], including the 1 ms spin precesion time and temporal width of the molecular pulse. This is accomplished by sending the detection laser through two different beam paths, each with one of two perpendicular linear polarizers. The two beam paths can be rapidly switched on and off with acousto-optic modulators.

The transparent electric field plates allow us to collect a large fraction of the solid angle of fluorescence from the molecules. Fluorescence travels through the field plates into an eight-lens system (four behind each plate) which focuses the light into an optical fiber bundle. The four bundles on each side are coupled into a fused quartz light pipe, which carries the fluorescence to a PMT (outside the magnetic shields). The net detection efficiency, including collection solid angle and detector quantum efficiency, is $\approx 1\%$. We typically register ≈ 1000 photon counts per molecule pulse. The PMT photocurrents are read as analog signals by a low-noise, high-bandwidth amplifier, and then sent to a 24-bit digitizer operating at 5 megasamples/s. The control and timing for all experimental parameters is managed by a single computer, and the timing jitter is less than one digitizer sampling period.

1. E. M. Purcell and N. F. Ramsey, "On the Possibility of Electric Dipole Moments for Elementary Particles and Nuclei," *Phys. Rev.*, vol. 78, p. 807, June 1950.
2. J. J. Hudson, D. M. Kara, I. J. Smallman, B. E. Sauer, M. R. Tarbutt, and E. A. Hinds, "Improved measurement of the shape of the electron.," *Nature*, vol. 473, pp. 493–6, May 2011.
3. I. B. Khriplovich and S. K. Lamoreaux, *CP Violation Without Strangeness*. Springer, 1997.
4. P. G. H. Sandars, "The Electric Dipole Moment of an Atom," *Physics Letters*, vol. 14, p. 194, Feb. 1965.
5. B. Regan, E. Commins, C. Schmidt, and D. DeMille, "New Limit on the Electron Electric Dipole Moment," *Physical Review Letters*, vol. 88, pp. 18–21, Feb. 2002.
6. D. M. Kara, I. J. Smallman, J. J. Hudson, B. E. Sauer, M. R. Tarbutt, and E. A. Hinds, "Measurement of the electron's electric dipole moment using YbF molecules: methods and data analysis," *New Journal of Physics*, vol. 14, p. 103051, Oct. 2012.
7. M. A. Player and P. G. H. Sandars, "An experiment to search for an electric dipole moment in the 3_2^P metastable state of xenon," *J. Phys. B*, vol. 3, pp. 1620–1635, 1970.
8. S. Bickman, P. Hamilton, Y. Jiang, and D. DeMille, "Preparation and detection of states with simultaneous spin alignment and selectable molecular orientation in PbO," *Physical Review A*, vol. 80, p. 023418, Aug. 2009.
9. S. Eckel, P. Hamilton, E. Kirilov, H. W. Smith, and D. DeMille, "Search for the electron electric dipole moment using Ω-doublet levels in PbO," *Physical Review A*, vol. 87, p. 052130, May 2013.
10. A. C. Vutha, W. C. Campbell, Y. V. Gurevich, N. R. Hutzler, M. Parsons, D. Patterson, E. Petrik, B. Spaun, J. M. Doyle, G. Gabrielse, and D. DeMille, "Search for the electric dipole moment of the electron

with thorium monoxide," *Journal of Physics B: Atomic, Molecular and Optical Physics*, vol. 43, p. 74007, Apr. 2010.
11. A. C. Vutha, B. Spaun, Y. V. Gurevich, N. R. Hutzler, E. Kirilov, J. M. Doyle, G. Gabrielse, and D. DeMille, "Magnetic and electric dipole moments of the $H^3\Delta_1$ state in ThO," *Physical Review A*, vol. 84, p. 034502, Sept. 2011.
12. S. E. Maxwell, N. Brahms, R. DeCarvalho, D. R. Glenn, J. S. Helton, S. V. Nguyen, D. Patterson, J. Petricka, D. DeMille, and J. M. Doyle, "High-Flux Beam Source for Cold, Slow Atoms or Molecules," *Physical Review Letters*, vol. 95, p. 173201, Oct. 2005.
13. N. R. Hutzler, M. F. Parsons, Y. V. Gurevich, P. W. Hess, E. Petrik, B. Spaun, A. C. Vutha, D. DeMille, G. Gabrielse, and J. M. Doyle, "A cryogenic beam of refractory, chemically reactive molecules with expansion cooling.," *Physical chemistry chemical physics : PCCP*, vol. 13, pp. 18976–85, Nov. 2011.
14. L. V. Skripnikov, A. N. Petrov, and A. V. Titov, "Theoretical study of ThO for the electron electric dipole moment search," *arXiv*, p. 1308.0414, Aug. 2013.
15. V. A. Dzuba, V. V. Flambaum, and C. Harabati, "Relations between matrix elements of different weak interactions and interpretation of the parity-nonconserving and electron electric-dipole-moment measurements in atoms and molecules," *Phys. Rev. A*, vol. 84, p. 052108, Nov 2011.
16. E. Kirilov, W. C. Campbell, J. M. Doyle, G. Gabrielse, Y. V. Gurevich, P. W. Hess, N. R. Hutzler, B. R. OLeary, E. Petrik, B. Spaun, A. C. Vutha, and D. DeMille, "Shot-noise-limited spin measurements in a pulsed molecular beam," *Physical Review A*, vol. 88, p. 013844, July 2013.
17. P. Hamilton, *Preliminary results in the search for the electron electric dipole moment in PbO*. PhD thesis, Yale University, 2010.
18. G. J. Feldman and R. D. Cousins, "Unified approach to the classical statistical analysis of small signals," *Physical Review D*, vol. 57, pp. 3873–3889, Apr. 1998.
19. J. H. Curtiss, "On the Distribution of the Quotient of Two Chance Variables," *The Annals of Mathematical Statistics*, vol. 12, pp. 409–421, Dec. 1941.
20. H. G. Berry, G. Gabrielse, and A. E. Livingston, "Measurement of the Stokes parameters of light.," *Applied optics*, vol. 16, pp. 3200–5, Dec. 1977.
21. W. Griffith, M. Swallows, T. Loftus, M. Romalis, B. Heckel, and E. Fortson, "Improved Limit on the Permanent Electric Dipole Moment of Hg199," *Physical Review Letters*, vol. 102, p. 101601, Mar. 2009.
22. S. Barr, "A Review of CP Violation in Atoms," *International Journal of Modern Physics A*, vol. 08, pp. 209–236, Jan. 1993.
23. M. Pospelov and A. Ritz, "Electric dipole moments as probes of new physics," *Ann. Phys.*, vol. 318, pp. 119–169, July 2005.
24. N. Arkani-hamed and S. Dimopoulos, "Supersymmetric Unification Without Low Energy Supersymmetry And Signatures for Fine-Tuning at the LHC,"
25. N. R. Hutzler, H.-I. Lu, and J. M. Doyle, "The buffer gas beam: an intense, cold, and slow source for atoms and molecules.," *Chemical Reviews*, vol. 112, pp. 4803–27, Sept. 2012.
26. R. A. Patten, "Michelson Interferometer as a Remote Gauge," *Applied Optics*, vol. 10, no. 12, pp. 2717–2721, 1971.
27. T. Hall, L.-S. Ma, M. Taubman, B. Tiemann, F. Hong, O. Pfister, and J. Ye, "Stabilization and frequency measurement of the I_2-stabilized nd:yag laser," in *Precision Electromagnetic Measurements Digest, 1998 Conference on*, pp. 151–152, 1998.
28. G. Edvinsson, A. Bornstedt, and P. Nylén, "Rotational Analysis for a Perturbed $^1\Pi$ state in ThO," *Ark. Phys.*, vol. 38, p. 193, 1968.
29. G. Edvinsson and A. Lagerqvist, "Two new band systems in ThO," *Physica Scripta*, vol. 41, pp. 316–320, 1990.
30. J. Paulovic, T. Nakajima, K. Hirao, R. Lindh, and P. A. Malmqvist, "Relativistic and correlated calculations on the ground and excited states of ThO," *J. Chem. Phys.*, vol. 119, no. 2, pp. 798–805, 2003.

AcknowledgementsPeople, NSF, NIST PMG

Author Contributions

Author Information The authors declare no competing financial interests. Correspondence and requests for materials should be addressed to XXX.